Roth, F., Dahm, T., Hainzl, S. (2017): Testing stress shadowing effects at the South American subduction zone. - *Geophysical Journal International*, *211*, 2, pp. 1272—1283.

DOI: http://doi.org/10.1093/gji/ggx362

Geophysical Journal International

Geophys. J. Int. (2017) **211,** 1272–1283
Advance Access publication 2017 August 26
GJI Seismology

doi: 10.1093/gji/ggx362

Testing stress shadowing effects at the South American subduction zone

F. Roth, T. Dahm and S. Hainzl

GFZ German Research Centre for Geosciences, D-14473 Potsdam, Germany. E-mail: hainzl@gfz-potsdam.de

Accepted 2017 August 24. Received 2017 August 22; in original form 2017 May 17

SUMMARY

The seismic gap hypothesis assumes that a characteristic earthquake is followed by a long period with a reduced occurrence probability for the next large event on the same fault segment, as a consequence of the induced stress shadow. The gap model is commonly accepted by geologists and is often used for time-dependent seismic hazard estimations. However, systematic and rigorous tests to verify the seismic gap model have often failed so far, which might be partially related to limited data and too tight model assumptions. In this study, we relax the assumption of a characteristic size and location of repeating earthquakes and analyse one of the best available data sets, namely the historical record of major earthquakes along a 3000 km long linear segment of the South American subduction zone. To test whether a stress shadow effect is observable, we compiled a comprehensive catalogue of mega-thrust earthquakes along this plate boundary from 1520 to 2015 containing 174 earthquakes with $M_w > 6.5$. In our new testing approach, we analyse the time span between an earthquake and the last event that ruptured the epicentre location, where we consider the impact of the uncertainties of epicentres and rupture extensions. Assuming uniform boundary conditions along the trench, we compare the distribution of these recurrence times with simple recurrence models. We find that the distribution is in all cases almost exponentially distributed corresponding to a random (Poissonian) process; despite some tendencies for clustering of the $M_w \geq 7$ events and a weak quasi-periodicity of the $M_w \geq 8$ earthquakes, respectively. To verify whether the absence of a clear stress shadow signal is related to physical assumptions or data uncertainties, we perform simulations of a physics-based stochastic earthquake model considering rate and state-dependent earthquake nucleation, which are adapted to the observations with regard to the number of events, spatial extend, size distribution and involved uncertainties. Our simulations show that the catalogue uncertainties lead to a significant blurring of the theoretically peaked distribution, but the distribution would be still distinguishable from the observed one for $M_w \geq 7$ events. However, considering the stress transfer to adjacent fault segments and heterogeneous instead of constant stress drop within the rupture zone can explain the observed recurrence time distribution. We conclude that simplified recurrence models, ignoring the complexity of the underlying physical process, cannot be applied for forecasting the $M_w \geq 7$ earthquake occurrence at this plate boundary.

Key words: South America; Earthquake interaction, forecasting, and prediction; Seismicity and tectonics; Statistical seismology; Subduction zone processes.

1 INTRODUCTION

The hypothesis of seismic gaps has been formulated since a long time. As early as the end of the 19th century, Gilbert (1884) already published a paper in which he formulated the idea that stress is built-up and released, and therefore it is not likely that an event occurs in the same area just after stress was decreased by a previous earthquake. This was well before the theory of plate tectonics was formulated and accepted. In view of plate tectonics, Scholz (1990, p. 260) defined a gap: under the assumption of plate motion being steady in time and continuous along a plate boundary as well as releasing a significant portion of stress seismically, it would be most likely that the segment which did not rupture for the longest time, has the highest probability to fail next.

Early observations of such a behaviour were reported by Fedotov (1965) for the northwestern Pacific, studying the gaps between the

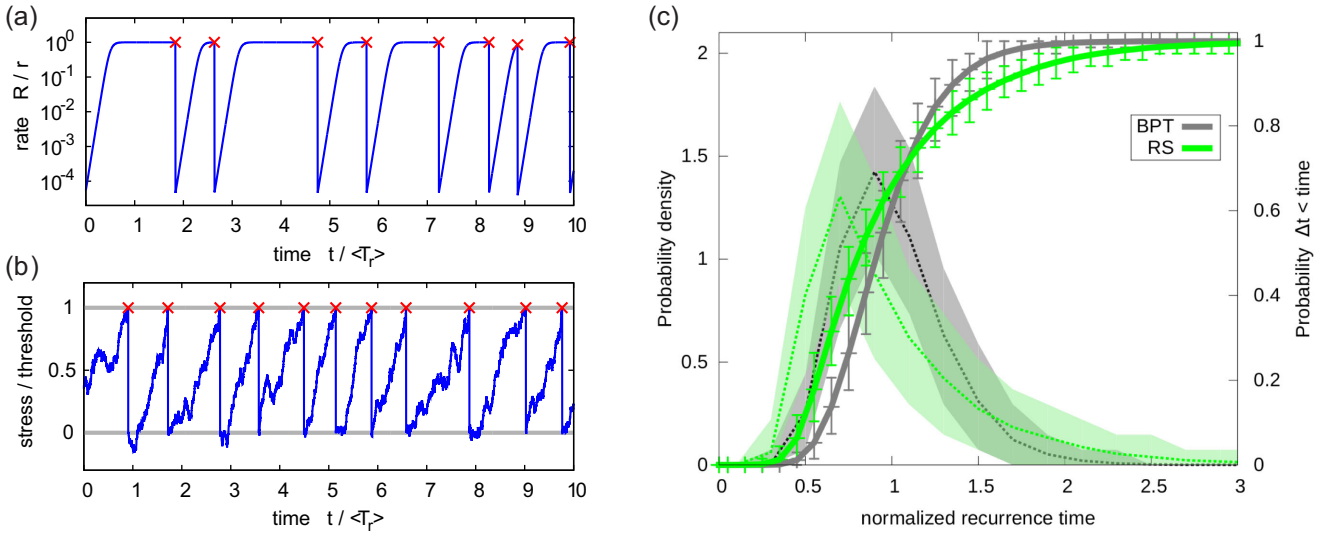

Figure 1. Simulations of recurrences on a single segment: (a) Earthquake rate as function of normalized time (divided by the average recurrence time $\langle T_r \rangle$) for an exemplary RS simulation with $r = 0.01$ yr^{-1}, $A\sigma = 0.1$ MPa, $t_a = 10$ yr and a stress drop of 1 MPa (see detailed description in Section 3.1). (b) Exemplary stress evolution of the Brownian oscillator leading to a BPT distribution with aperiodicity parameter 0.3. In both plots, red crosses indicate earthquake occurrences. (c) Corresponding cumulative distribution (cdf, scale on right) and probability density function (pdf, scale on left) of both model simulations. The results are shown for 1000 simulations of 68 recurrences as available in the case of the observed $M \geq 7.0$ record in Chile, where the shaded areas refer to the 90 per cent confidence interval, while curves refer to the mean values.

rupture zones of large shallow earthquakes along the arc before Japan, the Kuriles and Kamchatka. Other studies, especially covering the Chile subduction zone are of Mogi (1968), Sykes (1971), Kelleher (1972), Kelleher *et al.* (1973) and Nishenko (1985). For more references please see Rong *et al.* (2003). Perhaps the most comprehensive studies covering the whole of the circum-Pacific plate boundaries are those of McCann *et al.* (1979) and Nishenko (1991). McCann *et al.* (1979) provided the earthquake potential on the basis of time elapsed since the last large event, assuming that characteristic earthquakes occur quasi-periodically and that a mean recurrence time and its standard deviation can be estimated from the historical record of such events. Nishenko (1985) and Nishenko (1991) estimated the conditional probability for events filling the gap for 5 yr (1989–1994), 10 yr (1989–1999) and 20 year periods (1989–2009) based on a lognormal distribution approach. As far as statistically testable, the forecast of McCann *et al.* (1979) and the forecast of Nishenko (1991) were both rejected after their publication by Kagan & Jackson (1991, 1995) on the basis of the subsequent 10 yr and 5 yr of earthquake data, respectively. A follow-up study by Rong *et al.* (2003) statistically disproved the models based on an extended period of 20 and 10 yr, respectively. Kagan & Jackson (1991) suggested that large earthquakes occur predominantly in spatial and temporal clusters rather than quasi-periodically. To estimate conditional probabilities for the recurrence of earthquakes, they proposed an alternative approach which is solely based on the Poisson model (Kagan & Jackson 1995). In this model, earthquakes have no memory and the probability of an earthquake to occur in a given time interval from now is constant, independent on the time of the last event at this segment.

The statistical failure of the intuitively reasonable gap concept was somehow unexpected, since it would indicate that earthquakes have either no memory or that major earthquakes would even tend to occur in spatiotemporal clusters. This would have consequences on the way we estimate time-dependent seismic hazard. It would reduce the importance of historical and palaeoseismic earthquake data on the assessment of seismic hazard. It would also question the validity of physics-based models postulating the existence of long term stress shadows. One well-known example of those models is the Brownian oscillator leading the Brownian Passage Time (BPT) recurrence time distribution of earthquakes (Matthews *et al.* 2002), which is used for seismic hazard assessments, for example, in Taiwan (Wang *et al.* 2016). It assumes a fixed stress threshold and drop but a variable stress loading history modelled by a random walk with drift, where the degree of randomness correlates to the aperiodicity value (α = standard deviation divided by the mean) of the BPT distribution. Typical α-values used in applications are in the range between 0.2 and 0.8 which leads to a stress shadow effect and a quasi-periodic recurrence of the events. An example for $\alpha = 0.3$ is shown in Fig. 1. The rate and state (RS) model is a more general seismicity model which also predicts stress shadows. It is based on the stochastic response of the earthquake nucleation rate to a stressing history, where the experimentally observed rate- and state-dependent friction laws are taken into account (Dieterich 1994). For constant loading rate and stress drops, this model also predicts a quasi-periodic recurrence of the events. This is shown in Fig. 1 for a simulation of one fault segment with uniform stress drop.

Different reasons might explain why previous statistical tests rejected the gap model with high confidence. One reason might be the assumption that consecutive earthquakes rerupture the same fault segment with the same size, which does not account for the complexity of observed earthquake ruptures and the occurrence of secondary earthquakes which only release a small fraction of the accumulated stress at the plate interface. Thus we drop the assumption of characteristic earthquakes. In our study, subsequent ruptures are allowed to have only partial overlaps and varying sizes. To distinguish the tested model from the more strict gap model, we refer to it as stress-shadow model. Another reason for the previous failures of the gap model might be poor data sets of historical earthquakes and their errors. Historical earthquake catalogues have uncertainties in several parameters, which are difficult to

assess. The magnitude, epicentre and depth location, the extent of the rupture plane have often been estimated from different combinations of input data including intensity observations. It is sometime not even easy to verify that a major earthquake ruptured the plate interface along the subduction plate boundary, or might be related to the rupture in the overriding plate. Some of these uncertainties have been considered in previous studies. For instance, Rong *et al.* (2003) used three different catalogues for the period of their analysis (1978 June 1 to 1998 December 31) to take into account the magnitude uncertainty, containing events (i) $M_s \geq 7.0$ from PDE (National Earthquake Information Center 1999), (ii) $M_{other} > =7.0$ from other stations listed in the PDE catalogue, (iii) M_w calculated from the seismic moment given in the CMT catalogue (Dziewoński *et al.* 1981; Ekström *et al.* 2012).

Our study improves some of the shortcomings of previous testings. First, we constrain our analysis to a linear segment of the Nazca plate boundary with high, nearly homogeneous convergence rate, which allows a common analysis of all events on this lineament without a questionable predefinition of subsegments related to the recurrence of characteristic earthquakes. Second, the plate boundary under study includes the largest instrumentally recorded earthquake (i.e. M_W9.6 in Chile 1960) and several mega-thrust earthquakes in the recent past and historic times. Last not least, we adapt a completely new testing procedure, which considers uncertainties in different types of earthquake parameters and includes a comparison to the outcome of numerical RS-simulations of a similar long fault (3000 km) considering realistic uncertainties, stress transfer, and variable stress drops.

2 OBSERVATIONAL DATA

We study the historical record of major earthquakes along a 3000 km long linear part of South American plate boundary between 45°S and 15°S with rather homogeneous boundary conditions regarding the convergence rate and the dip angle of the subduction slab. This allows a common analysis of the earthquake activity over the whole length including the largest instrumentally recorded earthquake (i.e. M_w9.6 in Chile 1960) and several recent mega-thrust earthquakes from the last decade (Tocopilla 2007/11/14, M_{wp}7.9; Maule 2010/02/27, M_w8.8; Iquique 2014/04/01, M_w8.1; Illapel 2015/09/16, M_w8.2) together with several mega-thrust events of the last centuries (1575/12/16, M_s8.5; 1604/11/24, M_s8.7; 1647/05/14, M_s8.5; 1730/07/08, M_s8.8; 1751/05/25, M_s 8.5; 1784/05/13, M_s8.5; 1822/11/20, M_s8.5; 1868/08/13, M_s8.8; 1877/05/10, M_s8.8).

2.1 Data preparation

We consider historical earthquakes at the Chilean trench between 45°S and 15°S and 68.5°W and 74°W with hypocentres shallower than 70 km and used the most recent available data, especially concerning rupture length and position as well as magnitude. Epicentres and magnitudes of pre-instrumental earthquakes between 1500 and 1899 are taken from the CERESIS catalogue (Askew & Algermissen 1985; Giesecke *et al.* 2004). From 1900 to 2013 we use the ISC-GEM data (Storchak *et al.* 2013). Later earthquakes are included by hand, that is, for the 2014 Iquique earthquake using Geersen *et al.* (2015) and Schurr *et al.* (2014) and for the 2015 Illapel earthquake using Tilmann *et al.* (2016). We confine our study to earthquakes with intensity of 8 and higher or any magnitude value being equal or higher than 6.5. In the CERESIS catalogue before 1900, many events have no magnitude and no depth information. In this case, we convert the intensity to M_S using a depth-independent formula of Kárník (1969).

For events with moments not listed by other sources, we use M_w or M_e, and when neither of them was given, we determine M_w from M_s by calculating the static seismic moment via the relations of Di Giacomo *et al.* (2015).

The length and positions of rupture planes along the trench were taken from data collections of Beck *et al.* (1998), Comte *et al.* (1986), Comte & Pardo (1991) and Udías *et al.* (2012). The rupture length and location for recent strong events were taken from Barrientos & Ward (1990) for the M9.6 1960 Valdivia earthquake, Delouis *et al.* (1997) for the M7.6 1987 earthquake near Antofagasta, Ruegg *et al.* (1996) for the M8.0 1995 Antofagasta earthquake, Pritchard & Simons (2006) for the M9.6 1960 Valdivia earthquake, Chlieh *et al.* (2011) for the M8.4 2001 Arequipa earthquake, the rupture plane of which extends well into our area of investigation, Schurr *et al.* (2014) for the M7.9 2007 Tocopilla earthquake, Yue *et al.* (2014) for the M8.8 2010 Maule earthquake, Geersen *et al.* (2015) and Schurr *et al.* (2014) for the M8.1 2014 Iquique earthquake, and Tilmann *et al.* (2016) for the M8.2 2015 Illapel earthquake. In the case that the rupture length is not constrained by observations, we estimate rupture lengths from the scaling relation of Blaser *et al.* (2010) for dip-slip inter-plate earthquakes.

Based on Beck *et al.* (1998), we exclude the January 25, 1939 earthquake at 70.0°W, 24.5°S as a normal faulting event inside the hanging wall. Following Comte & Pardo (1991), we also exclude the earthquakes of April 22, 1870 at 68.9°W, 22.5°S, October 26, 1876 at 69.6°W, 22.1°S and January 23, 1878 at 69.5°W, 19.9°S as intra-plate events.

There is a wide variety of values given for event magnitudes. For instance, the CERESIS catalogue provides up to 4 magnitude and one intensity value. The ISC catalogue lists up to several dozens of magnitude values partially of different kind. To minimize saturation effects, we have chosen the maximum values. We end up with 174 earthquakes in the period 1520 to 2015 between 45°S and 15°S with $M_w > 6.5$, including 111 events with $M_w \geq 7$, 54 events with $M_w \geq 7.5$, and 29 earthquakes with $M_w \geq 8$. However, the catalogue is not homogeneous in space and time. To account for completeness, we consider the following two alternative data sets:

M7+: The $M_w \geq 7$ events which occurred between 40°S and 18°S in the last 200 yr.

M8+: The $M_w \geq 8$ events occurred between 42°S and 15°S in the last 500 yr.

Space time plots of the earthquake ruptures of both data sets are shown in Figs 2(a) and (b). We restrict the analysis of the $M_w \geq 7$ events to the last 200 yr, because the change point around 1815 in the number versus time plot (Fig. 2c) indicates that the catalogue misses many $M_w < 8$ events before. In contrast, the $M_w \geq 8$ data does not show any clear change point indicating an almost complete recording during the last 500 yr. Nevertheless, a partial incompleteness cannot be ruled out. In particular, the observed gap around 25°S before the year 1850 is likely related to some missed recordings in the Atacama desert. However, we have checked that our results are not affected by such a continuous data gap in the beginning of the data set (see Section 4 and Supporting Information). For the two time periods of the last 200 and 500 yr, Fig. 2(d) shows the frequency–magnitude distribution. The recordings in the last 200 yr can be well fitted by a Gutenberg–Richter distribution with $b = 0.75$ indicating the completeness of the M7+ data set. The observed b-value fits well in the range of b-values found for instrumentally recorded seismicity of subduction zones and thrust events (Schorlemmer *et al.* 2005; Nanjo *et al.* 2012; Schurr *et al.* 2014).

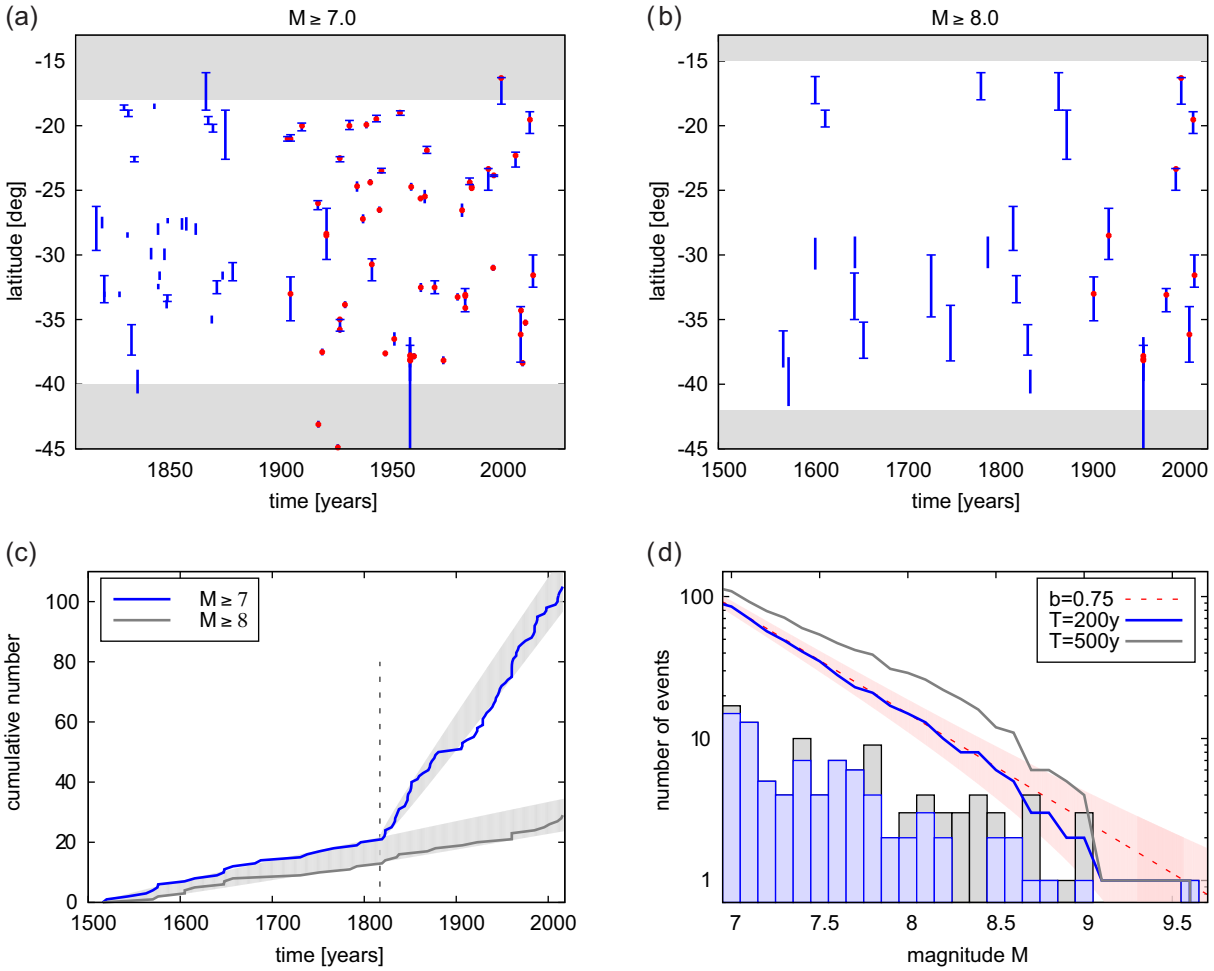

Figure 2. The rupture history of $M_w \geq 7.0$ (a) and $M_w \geq 8.0$ (b) subduction earthquakes in South America. Vertical lines refer to the rupture extension, where a missing horizontal bar indicates that this end is determined using the scaling relation of Blaser *et al.* (2010). Points mark the epicentres and activity in the grey shaded area is ignored in the analysis of the corresponding data sets M7+ and M8+. (c) The cumulative number of $M_w \geq 7.0$ (blue line) and $M_w \geq 8.0$ (grey line) events as function of time. The shaded grey areas refer to plus/minus one standard deviation of a Poisson process with a rate equal to the observed average rate of $M_w \geq 7.0$ and $M_w \geq 8.0$ events within the last 200 and 500 yr, respectively. The vertical dashed line indicates the starting time for the analysis of the $M_w \geq 7.0$ data set. (d) Frequency–magnitude distribution for the two time periods $T = 200$ and 500 yr: histogram (boxes) and cumulative distribution (lines). The red dashed line and shaded area refer to a Gutenberg–Richter distribution with $b = 0.75$ and plus/minus one standard deviation.

2.2 Uncertainties

The analysis of the recurrence times can be strongly affected by the large uncertainties of epicentre location and rupture extension of each event. To account for these uncertainties, we generate a large number of alternative realizations randomly sampled from probability distributions of the epicentre location and rupture extension. For that purpose, we assume the following distributions:

Epicentre. If it is instrumentally observed, the perturbed epicentre location is randomly chosen from a normal distribution with mean equal to the observed epicentre and a standard deviation of 10 km. For all other cases (historical records), the catalogue location defines the centroid location of the damages and thus the centre of the rupture. The true epicentre (nucleation point) of the earthquake is then assumed to be randomly located within the two rupture ends according to a normal distribution which is adapted to the empirically observed distribution of the relative position of the epicentres within ruptures (Mai *et al.* 2005). The adapted distribution is illustrated in the inset of Fig. 3.

Rupture ends. If reported in the catalogues, the uncertainty of the rupture ends is represented by a normal distribution with a standard deviation of 10 km. If only the epicentre or centroid location is recorded in the catalogue, the rupture ends are estimated in two steps: (i) The length of the ruptures are selected according to the empirical distribution of Blaser *et al.* (2010) for subduction events, which includes the spread of the empirical data for a given earthquake magnitude. (ii) The relative position of the epicentre within the rupture is randomly chosen from the normal distribution adapted to the empirical data (Mai *et al.* 2005, inset of Fig. 3).

In this way, we calculated 10 000 alternative Monte–Carlo (bootstrapped) versions of the earthquake catalogue. As examples, Fig. 3 shows five of such realizations for the case of the M8+ data set.

2.3 Analysis results

For each of the N earthquakes in one of the two data sets, we calculate the time interval Δt to the origin time of the last earthquake which ruptured the epicentre location. If no such event exists in the analysed data set, the event is ignored. This leads to a set of $N_{\Delta t}$ recurrence times with $N_{\Delta t} < N$. In the case of the M7+ data set, the number of recurrence times is $N_{\Delta t} = 68$ with an average of 26.8 yr,

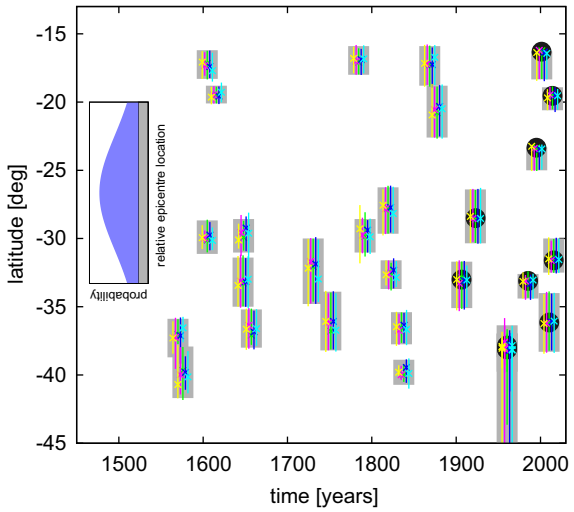

Figure 3. The $M_w \geq 8$ earthquake ruptures (bold grey bars) and epicentres (circles) in the catalogue in comparison to five bootstrapped catalogues with their rupture extensions (coloured bars) and epicentres (coloured crosses) which are randomly varied according to the assumed uncertainty distributions. The inset shows the form of the assumed probability density function in the case that epicentre information is missing in the original catalogue.

while the M8+ data set consists of 20 recurrences with an average of 117.9 yr. For a better comparison, we analyse the normalized recurrence times, that means the actual time divided by the average value, and determine the cumulative distribution function (cdf) and the probability density function (pdf). While the cdf(t) can be simply calculated by counting the number of recurrence times $\Delta t \leq t$ divided by the total number $N_{\Delta t}$, the pdf(t) has to be estimated by binning the time scale and dividing the observed number of recurrences in each bin by the bin width and the total number of recurrences. Due to the limited number of data, we choose a rather large bin width of 0.2 for the normalized recurrence times to ensure sufficient statistics. We calculate the cdf and pdf for the original catalogues and the bootstrapped ones in exactly the same way.

The result is shown in Fig. 4 for the M7+ and M8+ data sets. In addition to the result of the original data (green line), the blue shaded area refers to the 90 per cent confidence interval of the bootstrapped data; that means, the span between the 5 per cent smallest and the 95 per cent largest result of the 10 000 bootstrapped catalogues at each recurrence time. These results are compared to the mean and 90 per cent confidence interval in the case of a random occurrence of $N_{\Delta t}$ events in time (Poisson process). For that purpose, we also simulate 10 000 catalogues, where the recurrence times are randomly chosen from an exponential function (the pdf of a Poisson process). Fig. 4 shows that the uncertainties are large, particularly in the case of the M8+ data due to the small number of recurrences, and the distributions are mostly overlapping with the result for completely random data. However, some deviations can be seen. In particular, the M7+ data set shows some deviations from the Poissonian distribution at short times, while the larger recurrence times are less frequent than expected in a Poisson process, see especially Fig. 4(a). This indicates some degree of clustering in the data set. In contrast, the M8+ data set does not show any signal of clustering instead it shows a tendency for a quasi-periodic recurrence, see especially Fig. 4(d). However, the peak is not well separated from the distribution of random occurrences. To test whether the observed distribution is in agreement with Poisson process, we apply the Kolmogorov–Smirnov (KS) test. Here we use the Lilliefors-corrected test version since we estimate the mean rate of occurrences directly from the ensemble. The probability that the observed interevent times are the result of a Poisson process is 0.15 in the case of the M7+ data set and 0.013 for the M8+ events. Accounting for the involved uncertainties, we find that the hypothesis of a Poisson process can be rejected at a significance level of 0.05 only in 17 per cent of the M7+ bootstrapped catalogues. In contrast, for the same significance level, a majority of 86 per cent of the catalogues show significant deviations in the case of the M8+ events. Nonetheless, the Poisson hypothesis cannot be rejected for 14 per cent of the M8+ bootstrapped catalogues. This indicates the weakness of the non-random signals embedded in the M7+ and M8+ data sets. Whether the gap signal is just blurred because of the limited observation numbers and the large location uncertainties or the physical assumptions are wrong is explored in the following section by means of physics-based simulations.

3 COMPARATIVE ANALYSIS OF NUMERICAL SIMULATIONS

In the following, we perform numerical simulations of a simple physics-based stochastic earthquake simulator to quantify the effect of data uncertainties and simplified model assumptions. For a direct comparison with the observations, we run simulations of a 1-D fault with comparable length to the Chilean trench. The simulations are not intended to reproduce the details of real earthquake processes. However, they are based in a physically consistent way on the two fundamental assumptions of the stress-shadow model, a constant tectonic loading and stress drops related to earthquake occurrences, and account for the stochastic nature of earthquake nucleation and rupture processes which cannot be easily reproduced by deterministic models. To ensure the comparability to our observed data, the analysed simulations are constrained by the observations with regard to the number of recurrences and the size distribution.

3.1 Numerical simulations (RS model)

The applied model is the widely used stochastic model version for rate- and state-dependent frictional earthquake nucleation which has been introduced by Dieterich (1994). It is based on the velocity dependence and state dependence of the frictional strength observed in laboratory experiments (Linker & Dieterich 1992; Scholz 1998). The model assumes the existence of a population of independent nucleation sites which leads to its stochastic nature. In this model, the seismicity rate R is inversely proportional to the state variable γ describing the creep velocities on the faults, namely,

$$R(t) = \frac{r}{\dot{\tau}\gamma(t)}\,, \tag{1}$$

where r is the stationary earthquake background rate and $\dot{\tau}$ the tectonic loading rate. The evolution of the state variable as a function of time t and shear stress τ is given by $\mathrm{d}\gamma = (\mathrm{d}t - \gamma\,\mathrm{d}\tau)/(A\sigma)$, with σ being the effective normal stress and A a dimensionless fault constitutive parameter usually $\sim$0.01 (Dieterich 1994; Dieterich *et al.* 2000).

For a single stress step the change $\Delta\tau$ occurring in a period of stationary seismicity rate r, the evolution law yields an earthquake rate

$$R(t) = \frac{r}{1 + \left(\mathrm{e}^{-\frac{\Delta\tau}{A\sigma}} - 1\right)\mathrm{e}^{-\frac{t}{t_a}}} \tag{2}$$

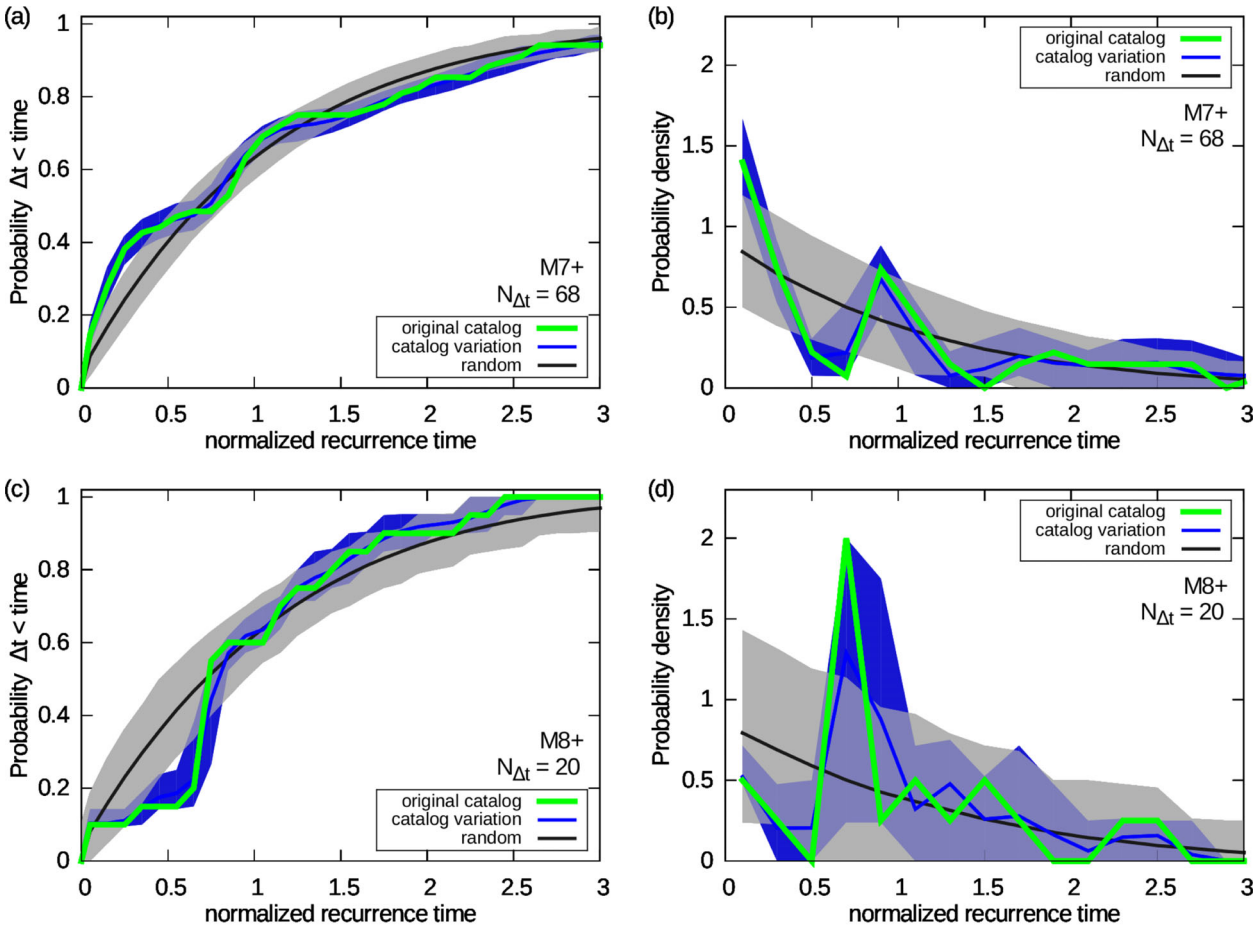

Figure 4. The normalized distribution of the observed recurrences in the case of the M7+ (a,b) and M8+ (c,d) data set. The left column shows the cumulative distribution (cdf) and the right column the probability density (pdf) function of the recurrence times, respectively. The shaded areas refer to the 90 per cent confidence interval, while curves refer to the mean values. The results for the original data are shown as green lines. For comparison, the results for the data sets with resampled locations from the uncertainty distributions are shown in blue and the results for a Poisson process are shown in grey.

as a function of the elapsed time t after the stress step, where t_a is the aftershock duration, $t_a \equiv A\sigma/\dot{\tau}$. For positive stress steps, the triggered excess rate is equal to the Omori–Utsu decay with $p = 1$ on short times, but with an exponential roll-off at time t_a (Dieterich 1994; Cocco *et al.* 2010). For negative stress steps (stress drops), the seismicity rate is immediately suppressed by a factor $\exp(-|\Delta\tau|/A\sigma)$ and stays low for a duration significantly longer than t_a. For stress drops $|\Delta\tau| \gg A\sigma$, eq. (2) can be approximated by $R(t) = r/(1 + \exp(-[\Delta\tau + \dot{\tau}t]/A\sigma))$ which leads to a life time t_q of the quiescence equal to $t_q = t_a + |\Delta\tau|/\dot{\tau}$. For multiple stress steps, the state variable γ and thus the rate $R(t)$ can be calculated by iteration (Hainzl *et al.* 2010).

As for the observed data, we only consider trench parallel distances assuming full rupturing of the seismogenic zone. The earthquake generation is simulated over a length of 3000 km length, where the fault is discretized into bins of 1 km. After each earthquake, γ is iterated and the time to the next failure is calculated at each bin. The location with the minimum time becomes the epicentre of the next earthquake. Its size is randomly chosen in the magnitude range between 7.0 and 9.5 according to a Gutenberg–Richter distribution with a b-value of 0.75 in agreement with our observed data set (see Fig. 2d). Dependent on its magnitude, the length of the ruptures are selected according to the empirical relations of Blaser *et al.* (2010). The rupture can be unilateral or bilateral. This is decided by taking the position of the epicentre randomly from a normal distribution which is adapted to the empirically observed distribution of the relative epicentre position within ruptures (Mai *et al.* 2005, see inset of Fig. 3). The size of the rupture does not depend on the rate variation along the trench and the rupture can propagate into neighbouring regions recently ruptured. Within the resulting rupture extension along trench, all locations experience a stress drop taken from a normal distribution with mean value of 1 MPa and a standard deviation $\sigma_{\Delta\tau}$. For $\sigma_{\Delta\tau} > 0$, the stress change can be locally positive although the average value is negative, which can trigger aftershocks (Marsan 2006). This can account in a simplified way for the geometrical heterogeneity and slip variability of observed earthquake ruptures. Because our simple 1-D approach does not explicitly model the depth extend of ruptures, $\sigma_{\Delta\tau} > 0$ can somehow account for ruptures which not break the full seismogenic depth leading to stress loads on the lower or upper seismogenic part within the trench parallel extension of the rupture, where subsequent events can nucleate with increased probability. Furthermore, we consider, if stated, positive stress transfer to adjacent fault segments. We implement a stress transfer function, $\Delta\mathrm{CFS}(r) = |\Delta\tau|(1 + r/l)^{-3}$, which depends on the distance r to the rupture and decays in the far field according to r^{-3} in agreement with the static stress of a point source. The intrinsic length scale is assumed to be proportional to the rupture length, $l = 0.1L$. Thus the stress increases close to the rupture by almost the same amount as it drops within the rupture on average.

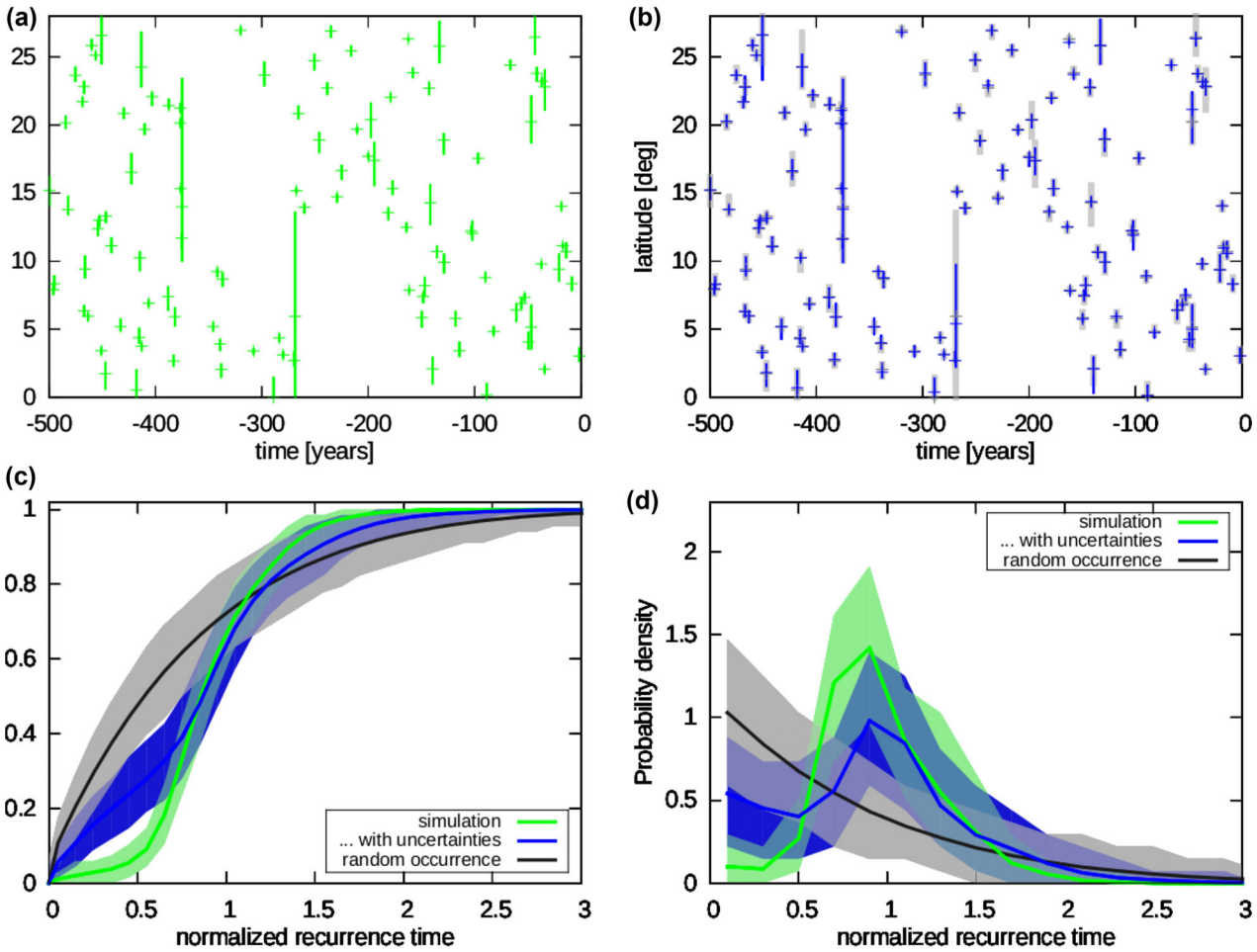

Figure 5. Examples and results of numerical simulations of the RS model with constant stress drop ($\sigma_{\Delta\tau} = 0$) and no stress transfer: (a) Example of a simulated rupture history of $M \geq 7$ events, where vertical lines and crosses refer to the true rupture extensions and epicentres. (b) Example of a perturbed rupture history (blue lines and crosses) for the same example, where uncertainties are added in accordance to the assumed uncertainties of the empirical catalogue data. For comparison, the true values are shown in grey. (c) The cumulative distribution (cdf) and (d) the probability density (pdf) function of the recurrence times: The shaded areas refer to the 90 per cent confidence interval, while curves refer to the mean values. The result for 100 catalogues without location uncertainties (one example shown in a) are presented in green. For comparison, the results for the simulated catalogues including uncertainties (one example shown in b) are presented in blue and the results for a Poisson process are shown in grey.

The rate-state parameters are set to values in the centre of previously inverted parameters (Hainzl *et al.* 2010), namely $t_a = 10$ yr and $A\sigma = 0.1$ MPa. The background rate for $M \geq 7$ events occurring at the whole fault is set to 10 events per year, which leads to an average rate of 0.23 $M \geq 7$ yr^{-1}, if stress transfer is ignored. The difference between the unperturbed rate r and the actual average rate is due to the stress shadow effect of the earthquakes. To avoid any transient effects, we removed the first 10 000 yr of each simulation. One example of such a simulation is shown in Fig. 5(a) for the case of a uniform stress drop ($\sigma_{\Delta\tau} = 0$). This plot is equivalent to the presentation of the observed data in Figs 2(a) and (b). Two clear periods of quiescence are observed after the major events, while the stress shadow effect is less obvious in the case of the other events.

To ensure the same statistics in the observed and simulated data sets, we use the same number of recurrence times for the analysis, namely $N_{\Delta t} = 68$ for $M \geq 7$ events. The same degree of information about the rupture extension and epicentre location are applied for the simulated catalogues; that means, for example, for the first events we ignore the true epicentre position and use only the centroid location as assumed for the historic earthquakes. Uncertainties of rupture and epicentre locations are accounted for by the same bootstrapping approach as for the observed data (see Section 2.2). Fig. 5(b) shows an example of a bootstrapped version for the specific simulation in Fig. 5(a).

3.2 Model results

The recurrence time distribution is analysed for 100 numerical simulations with each 100 bootstrapped versions. At first, we want to analyse the effect of the small sample size and the assumed location uncertainties on the result of our model simulations. For that purpose, we first assume a uniform stress drop ($\Delta\tau = 1, \sigma_{\Delta\tau} = 0$) and ignore positive stress transfers to adjacent segments. The resulting recurrence time distributions are shown for the $M \geq 7$ events in Figs 5(c) and (d). Green colours refer to the result for the simulation without uncertainties, while blue colours correspond to the results for the catalogues with uncertainties similar to the observed data set. These results are compared to the corresponding result for completely random occurrences (Poisson process) with the same number of events (grey). In all cases, the shaded areas refer to the 90 per cent confidence interval of the results. The result of the simulations, where uncertainties are ignored, significantly deviates from

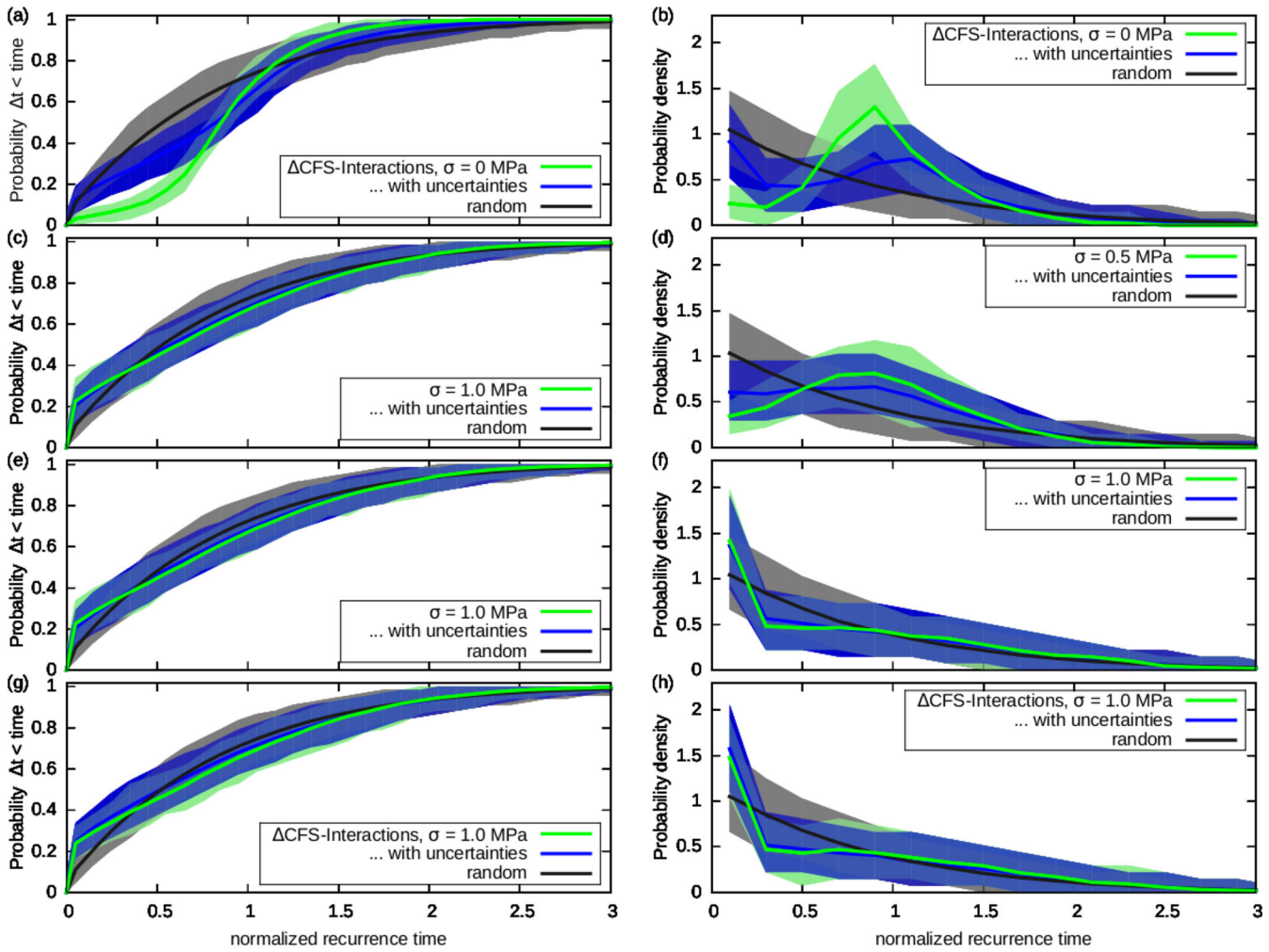

Figure 6. The cumulative (cdf, left column) and probability density (pdf, right column) function of the recurrence times in the space-time RS model, where stress transfer to adjacent fault segments is considered or/and the stress drops are variable. (a,b) Stress transfer is considered but the stress drop is uniform. (c–h) The stress drop is variable where its value in each bin of 1 km located inside a rupture is independently taken from a normal distribution with a mean of 1 MPa and standard deviation of 0.5 MPa (c,d) and 1.0 MPa (e–h). While in (c–f), no stress transfer is considered, it is taken into account in (g,h). The result for 100 simulations (without location uncertainties) of 68 recurrences is shown in green. For comparison, the corresponding results for the bootstrapped catalogues are presented in blue and for a Poisson process are shown in grey.

random occurrences in showing a clear peak, although the small sample size leads to a quite large variability. The KS-test yields a probability (p-value) that the observed interevent times are the result of a Poisson process of only 2×10^{-4}. Accounting for the involved uncertainties strongly smears the results and the final result becomes much closer to a random distribution. This happens because of the wrong or missed association of epicentres to previous ruptures at the same place. As a result, the peak in the pdf becomes less significant, broader, and slightly shifted to larger values. In addition, short artificial recurrence times are detected which are related to a false association of a precursory rupture at the epicentre location. The data sets with uncertainties lose some of its resolving power to proof the stress-shadow model against a Poissonian occurrence of earthquakes. This is verified by the KS-test which yields a median p-value of 0.006, while 14 per cent of the bootstrapped catalogues have insignificant p-values larger than 0.05. Additionally, we compare the simulated and observed data sets. The two sample KS-test confirms the visual impression that the simulations are significantly different from the observed M7+ data set. The probability that that both data sets stem from the same distribution is only 7×10^{-4} and only 5 per cent of the bootstrapped simulations have p-values larger than 0.05. In contrast, the difference of the simulations to the observed M8+ data is almost insignificant. The median p-value for the difference between bootstrapped catalogues and the M8+ data is 0.33 and more than 90 per cent of the bootstrapped simulations have insignificant values ($p > 0.05$).

For simplicity, we have ignored so far stress transfer to adjacent fault segments and any heterogeneity of the stress drop within the rupture. However, both phenomena are well known from observations (Stein 1999; Mai & Beroza 2002, etc.) and might be responsible for the observed discrepancy between the empirical data and the simulations. At first, we analyse the effect of stress transfers, while stress drop within the rupture remains uniform. The corresponding result is shown in Figs 6(a) and (b). For the case of the simulated catalogues without uncertainties, the resulting recurrence time distribution is almost identical to the case without any stress transfer. This is expected because the events triggered by the stress transfer nucleate outside of the rupture area. Thus they do not count as a recurrent rupture. In contrast, these triggered events might be falsely identified as nucleating within the previous

rupture zone, if the location uncertainties are considered. Therefore, the recurrence time distribution of the bootstrapped catalogues are showing an increased number of very short recurrences, somehow similar to the observed one for the M7+ data set. However, the peak of the quasi-periodic recurrence is still obvious. Now we also consider the effect of spatially heterogeneous stress drops. Figs 6(c)–(f) show the results for $\sigma_{\Delta\tau} = 0.5$ and 1 MPa, ignoring the effect of stress transfers, while Figs 6(g) and (h) refer to simulations with $\sigma_{\Delta\tau} = 1$ MPa and stress transfers. Already moderate stress drop variability ($\sigma_{\Delta\tau} = 0.5$ MPa) leads to a significantly reduced and broadened peak in the pdf. Additionally, short recurrence times occur in the model simulations because of the random occurrence of local patches with positive stress changes within the rupture which foster the occurrence of subsequent events at the same location leading to local event clustering. This tendency is strongly enhanced in the case of $\sigma_{\Delta\tau} = 1$ MPa. In this case, approximately 16 per cent of the patches within an earthquake rupture experience on average positive instead of negative stress changes due to the assumed heterogeneous earthquake slip. This percentage is enough to completely erase the peak in the pdf related to a quasi-periodic recurrence. Instead, enhanced short-time clustering dominates the occurrence similarly to the result for the observed M7+ data set. The KS-test confirms these results: For $\sigma_{\Delta\tau} = 0.5$ MPa, the median p-value of the test against the Poisson model is 0.035 with a 90 per cent confidence interval of [0.0008, 0.23] indicating that the simulations can be distinguished from a Poisson process but with rather low significance. The KS-comparison of the simulated recurrences with the observed recurrence time distribution of the data set yields more significant differences with a median value of $p = 0.01$ and a confidence interval of [0.001, 0.06]. This result changes for $\sigma_{\Delta\tau} = 1$ MPa. In this case, the simulations cannot be distinguished from a Poissonian process ($p = 0.15$ [0.0002, 0.61]) and not from the observed distribution ($p = 0.18$ [0.04, 0.54]). Thus, our model simulations suggest that variable stress can explain the observed recurrences in Chile. In particular, the stress drop variability within the rupture zone is found to be more decisive for the pattern of the recurrence distribution than positive stress transfer to neighbouring fault segments.

Although the result for the observed M8+ data set (Figs 4c and d) looks somehow similar to the simulation results for $\sigma_{\Delta\tau} = 0.5$ MPa (Figs 6c and d), the number of recurrences is too small to explore this in more detail. In particular, the KS-test for simulations of $N_{\Delta t} = 20$ recurrences of $M \geq 8$ events does not indicate for any $\sigma_{\Delta\tau}$-value (0.5, and 1 MPa) a statistical difference neither to a Poissonian process nor to the observed M8+ recurrences. The median p-values are in all cases greater than 0.1.

4 DISCUSSION

The papers by Kagan & Jackson (1991, 1995) concluded that large earthquakes at plate boundary occur purely randomly and have no memory until the occurrence of the previous earthquake rupturing the event. The predictions of previous time-dependent earthquakes occurrence models by Nishenko (1991) were disproved in these papers. One possible reason of this failure of the gap model could be the strong assumption made by previous applications, namely the recurrence of a characteristic earthquake which releases the stress always in the same fault segment. This requires persistent segment boundaries which prevent ruptures extending into neighbouring fault regions. While such boundaries might exist in some places (Victor *et al.* 2011), this assumption is generally not based on observational evidence. In fact, rupture nucleation and termination seems to be mostly of stochastic nature associated to a Gutenberg-Richter type size distribution and variable nucleation sites. In our new testing approach, we have thus relaxed this assumption by considering the time interval between an earthquake and the last rupture which released the stress at the epicentre location. Because this is a relative measure, the assumption of recurrences of characteristic earthquakes is not required but also not prohibited. However, we come to a similar conclusion as Kagan & Jackson (1991, 1995) and cannot find a clear stress shadow effect corresponding to a period of reduced probability for a subsequent $M_w \geq 7$ event at the collinear portion of the plate boundary in Chile.

By means of numerical simulations of the RS model with constant stress drop, we find that this observation cannot be fully explained by insufficient sample size or uncertainties. One reason could be missing earthquakes in the empirical catalogue or systematic biased magnitudes of historic events. A partial incompleteness of our data set cannot be ruled out. In particular, the observed gap around latitude 25°S before the year 1850 (Figs 2a and b) is likely related to some missed recordings in the Atacama desert. However, we have checked by means of numerical simulations (introduced in Section 3.1) that such a continuous data gap in the beginning of the data set has no significant influence on the results. The corresponding analysis is presented in the Supporting Information (Fig. S1). In the Supporting Information, we also analyse the effect of a systematic magnitude bias of historic events. The major change of the worldwide seismic network in the mid of the previous century lead to some apparent changes in seismicity (Hough 2013). In particular, the lack of instrumental recordings might lead to missing or underestimated earthquake magnitudes in sparsely populated areas and offshore regions. Our sensitivity analysis of earthquake catalogues where pre-1950 event magnitudes are artificially increased by increments of 0.1, 0.2, or 0.3 indicates that the results discussed for the original catalogue are robust (see Supporting Information Figs S2 and S3).

This leads to the conclusion that either the stress-shadow model does not match the underlying physics, or the assumptions of the seismic recurrence models are still too simple. The simplifying aspects in our method include (i) the assumption that the earthquakes rupture the major part of the seismogenic zone, (ii) the assumption that the stress drop during an event is homogeneous and (iii) that the stress build-up is homogeneous at constant rate and that inhomogeneous coupling and creep plays a minor role to describe seismic cycles. All this assumptions are likely not valid. In particular, assumption (i) related to our 1-D approach might be reasonable for $M_w \geq 8$ events but not for all $7 \leq M_w < 8$ earthquakes (Lay *et al.* 2012). If an earthquake ruptures only a part of the seismogenic width, the unbroken part will experience a stress increase and will break with a higher probability in the near future. This leads to an apparent re-rupturing of the same portion of the fault in our 1-D analysis resulting in a pdf indicating clustering as found for the observed M7+ data set. This would also explain the absence of clustering in the $M8+$ data set, where earthquakes are likely rupturing the whole seismogenic width. However, the M8+ data base of historic earthquakes is just too small to show very significant differences to a Poisson process, as demonstrated by our numerical simulations based on the physics of the gap theory (see Section 3.2). Palaeoseismic data are thus essential to test the occurrence of M8+ events. The second assumption (ii) is closely related to the first one, because heterogeneous slip can also lead to stress loads within the trench-parallel rupture extension. In a simplified way, we have tested the effect of heterogeneities related to (i) and (ii) in our numerical simulations by accounting for spatially random

stress drops which are chosen from a normal distribution with mean of 1 MPa and a standard deviation of $\sigma_{\Delta\tau} = 0$, 0.5 or 1 MPa. As shown in Section 3.2, the introduction of this variability can explain the observed recurrence time distributions.

Additional heterogeneity, for example, related to different average drops of the earthquakes as well as spatially and temporally varying loading and coupling conditions are expected to further randomize the results. Recent studies show that coupling is heterogeneous along strike (Metois *et al.* 2016). In principle, our analysis approach could account for variations of the coupling strength along strike by rescaling the local time scale (dividing the original time by the coupling coefficient). However, the uncertainties of the inversions of interseismic geodetic data are still very high. Furthermore, the data represent only a short portion of the seismic cycle and coupling might vary with time (Melnick *et al.* 2017). For simplification, we have thus assumed in our study that coupling at the earthquake hypocentres is constant along strike. This might be a good first-order approximation, because the study of Metois *et al.* (2016) also shows that a fully coupled zone (with variable width) exists almost continuously along strike. In addition, Ruegg *et al.* (2009) conclude that the interseismic deformation between 35.2°S and 38°S can be modelled to first order assuming an elastic rheology, a 100 per cent coupling and a constant locking depth at 60 km. Assuming that the major events are driven by the failure of this coupled zone, our model assumption of a uniform loading rate is reasonable. The new geodetic measurements provide us with a wealth of information about the present day stress build-up and release in dependence of strike and depth (e.g. Schurr *et al.* 2014; Tilmann *et al.* 2016; Frank *et al.* 2017; Melnick *et al.* 2017; Poli *et al.* 2017). In principle, the resulting detailed slip distributions offer the possibility for 2-D studies which could overcome some problems of our simple 1-D approach and likely lead to more positive test results. However, the uncertainties of these data and, even more importantly, their limited time coverage spanning only the last few decades do not allow so far the test of statistical recurrence models built on them.

5 CONCLUSIONS

Previous statistical tests indicated that the gap model fails to reproduce observed data (Kagan & Jackson 1991, 1995; Rong *et al.* 2003), which might be related to data limitations and uncertainties but also to wrong assumptions. One questionable assumption of the classical gap model is that characteristic earthquakes occur quasi-periodically at the same fault segment which requires persistent fault segmentation. In this paper, we have thus tested the stress-shadow model, a weaker version of the gap model, where future events are not necessarily bounded in their sizes and locations to fixed segments. For this purpose, we perform a common analysis of a comprehensive catalogue of shallow mega-thrust earthquakes along a 3000 km long linear segment at the Chilean trench which is assumed to have approximately homogeneous boundary conditions. The catalogue is found to be complete for earthquakes with $M_w \geq 7$ in the last 200 yr (89 events), and $M_w \geq 8$ in the last 500 yr back to the middle age in 1500 (29 events). Additionally, we have included measures of uncertainties for the epicentre location and the rupture ends. Our new approach estimates the recurrence time distributions for earthquake ruptures distributed over the whole length of the plate boundary accounting for their real rupture sizes. The assumption of the recurrence of characteristic earthquakes and a geological segmentation of the plate boundary is allowed but not required for our testing approach.

Our test shows that the observed recurrence time distribution is close to an exponential distribution related to a Poissonian process. However, the $M_w \geq 7$ events show some tendency for clustering, while the mega-thrust events with $M_w \geq 8$ indicate some tendency for a quasi-periodic recurrence. Our tests of numerical simulations of the RS model indicate that the observations for $M_w \geq 7$ events cannot be alone explained by location uncertainties or an insufficient database. Our results indicate that the assumption of uniform stress drops is invalid and leads to biased results. Accounting for the variability of stress changes, which is expected due to stress transfer, variable slip distributions, and geometrical complexity of real earthquake ruptures, leads to simulations in accordance with the observations. Thus our results show that the 1-D stress-shadow model, although likely based on valid physical mechanisms, might only be applicable to mega-thrust events but cannot be applied with simplified assumptions to model the recurrences of $M_w \geq 7$ events. A better knowledge of stress drop heterogeneities is important to implement physics-based, time-dependent seismic hazard models.

ACKNOWLEDGEMENTS

We are grateful to Piero Poli, Sandy Steacy and two anonymous reviewers for their very helpful comments. Discussions in sections 2.1 and 2.6 of GFZ and within the IPOC group improved the sharpness of our study. We thank Regina Milkereit for support in the layout of figures.

REFERENCES

Askew, B.L. & Algermissen, S.T., 1985. Catalog of earthquakes for South America: hypocenter and intensity data, (4–7c), in *Catálogo de Terremotos para América del Sur,* vol. 4, 269 pp., eds Askew, B. & Algermissen, S. T., CERESIS.

Barrientos, S.E. & Ward, S.N., 1990. The 1960 Chile earthquake: inversion for slip distribution from surface deformation, *Geophys. J. Int.,* **103,** 589–598.

Beck, S., Barrientos, S., Kausel, E. & Reyes, M., 1998. Source characteristics of historic earthquakes along the central Chile subduction zone, *J. South Am. Earth Sci.,* **11**(2), 115–129.

Blaser, L., Krüger, F., Ohrnberger, M. & Scherbaum, F., 2010. Scaling relations of earthquake source parameter estimates with special focus on subduction environment, *Bull. seism. Soc. Am.,* **100**(6), 2914–2926.

Chlieh, M. *et al.*, 2011. Interseismic coupling and seismic potential along the Central Andes subduction zone, *J. geophys. Res.,* **116,** B12405, doi:10.1029/2010JB008166.

Cocco, M., Hainzl, S., Catalli, F., Enescu, B., Lombardi, A.M. & Woessner, J., 2010. Sensitivity study of forecasted aftershock seismicity based on Coulomb stress calculation and rate- and state-dependent frictional response, *J. geophys. Res.,* **115,** B05307, doi:10.1029/2009JB006838.

Comte, D. & Pardo, M., 1991. Reappraisal of great historical earthquakes in the northern Chile and southern Peru seismic gaps, *Nat. Hazards,* **4,** 23–44.

Comte, D., Eisenberg, A., Lorca, E., Pardo, M., Ponce, L., Saragoni, R., Singh, S.K. & Suárez, G., 1986. The 1985 central Chile earthquake: a report of previous great earthquakes in the region, *Science,* **233,** 449–452.

Delouis, B. *et al.*, 1997. The $M_w = 8.0$ Antofagasta (northern Chile) earthquake of 30 July 1995: a precursor to the end of the large 1877 gap, *Bull. seism. Soc. Am.,* **87**(2), 427–445.

Dieterich, J.H., 1994. A constitutive law for rate of earthquake production and its application to earthquake clustering, *J. geophys. Res.,* **99,** 2601–2618.

Dieterich, J.H., Cayol, V. & Okubo, P., 2000. The use of earthquake rate changes as a stress meter at Kilauea volcano, *Nature,* **408,** 457–460.

Di Giacomo, D., Bondár, I., Storchak, D.A., Engdahl, E.R., Bormann, P. & Harris, J., 2015. ISC-GEM: Global Instrumental Earthquake Catalogue (1900–2009), III Re-computed M_S and M_b, proxy M_w, final magnitude composition and completeness assessment, *Phys. Earth planet. Inter.,* **239,** 33–47.

Dziewoński, A.M., Chou, T.-A. & Woodhouse, J.H., 1981. Determination of earthquake source parameters from waveform data for studies of global and regional seismicity, *J. geophys. Res.,* **86,** 2825–2852.

Ekström, G., Nettles, M. & Dziewoński, A.M., 2012. The global CMT project 2004-2010: centroid-moment tensors for 13,017 earthquakes, *Phys. Earth planet. Inter.,* **200–201,** 1–9.

Fedotov, S.A., 1965. Regularities in the distribution of strong earthquakes in Kamchatka, the Kuriles, and northeastern Japan, *Trudy Inst. Fiz. Zemli Akad. Nauk SSSR,* **36,** 66–93, In Russian.

Frank, W.B., Poli, P. & Perfettini, H., 2017. Mapping the rheology of the Central Chile subduction zone with aftershocks, *Geophys. Res. Lett.,* **44,** 5374–5382.

Geersen, J., Ranero, C.R., Barckhausen, U. & Reichert, C., 2015. Subducting seamounts control interplate coupling and seismic rupture in the 2014 Iquique earthquake area, *Nat. Commun.,* **6,** 8267, doi:10.1038/ncomms9267.

Giesecke, A., Capera, A.A.G., Leschiutta, I., Migliorini, E. & Valverde, L.R., 2004. The CERESIS earthquake catalogue and database of the Andean Region: background, characteristics and examples of use, *Ann. Geophys.,* **47**(2–3), 421–435.

Gilbert, G.K., 1884. A theory of earthquakes, *Am. J. Sci., 3rd ser.,* **27,** 49–53.

Hainzl, S., Steacy, S. & Marsan, D., 2010. Seismicity models based on Coulomb stress calculations, *Community Online Resource for Statistical Seismicity Analysis,* doi:10.5078/corssa-32035809. Available at: http://www.corssa.org.

Hough, S., 2013. Missing great earthquakes, *J. geophys. Res.,* **118,** 1098–1108.

Kagan, Y.Y. & Jackson, D.D., 1991. Seismic Gap hypothesis: ten years after, *J. geophys. Res.,* **96,** 21 419–21 431.

Kagan, Y.Y. & Jackson, D.D., 1995. New seismic gap hypothesis: five years after, *J. geophys. Res.,* **100,** 3943–3959.

Kárník, V., 1969. *Seismicity of the European Area, Part I,* Reidel Publ. Co..

Kelleher, J.A., 1972. Rupture zones of large American earthquakes and some predictions, *J. geophys. Res.,* **77,** 2087–2103.

Kelleher, J.A., Sykes, L. & Oliver, J., 1973. Possible criteria for predicting earthquake locations and their application to major plate boundaries of the Pacific and the Caribbean, *J. geophys. Res.,* **78**(14), 2547–2585.

Lay, T., Kanamori, H., Ammon, C.J., Koper, K.D., Hutko, A.R., Ye, L., Yue, H. & Rushing, T.M., 2012. Depth-varying rupture properties of subduction zone megathrust faults, *J. geophys. Res.,* **117,** B04311, doi:10.1029/2011JB009133.

Linker, M.F. & Dieterich, J.H., 1992. Effects of variable normal stress on rock friction—observations and constitutive-equations, *J. geophys. Res.,* **97**(B4), 4923–4940.

Mai, P.M. & Beroza, G.C., 2002. A spatial random field model to characterize complexity in earthquake slip, *J. geophys. Res.,* **107**(B11), 2308, doi:10.1029/2001JB000588.

Mai, P.M., Spudich, P. & Boatwright, J., 2005. Hypocenter locations in finite-source rupture models, *Bull. seism. Soc. Am.,* **95**(3), 965–980.

Marsan, D., 2006. Can coseismic stress variability suppress seismicity shadows? Insights from a rate-and-state friction model, *J. geophys. Res.,* **111,** B06305, doi:10.1029/2005JB004060.

Matthews, M.V., Ellsworth, W.L. & Reasenberg, P.A., 2002. A Brownian model for recurrent earthquakes, *Bull. seism. Soc. Am.,* **92**(6), 2233–2250.

McCann, W.R., Nishenko, S.P., Sykes, L.R. & Krause, J., 1979. Seismic gaps and plate tectonics: seismic potential for major boundaries, *Pure appl. Geophys.,* **117,** 1082–1147.

Melnick, D., Moreno, M., Quinteros, J., Baez, J.C., Deng, Z., Li, S. & Oncken, O., 2017. The super-interseismic phase of the megathrust earthquake cycle in Chile, *Geophys. Res. Lett.,* **44,** 784–791.

Metois, M., Vigny, C. & Socquet, A., 2016. Interseismic coupling, megathrust earthquakes and seismic swarms along the Chilean subduction zone (38°S–18°S), *Pure appl. Geophys.,* **173,** 1431–1449.

Mogi, K., 1968. Sequential occurrences of recent great earthquakes, *J. Phys. Earth,* **16**(1), 30–36.

Nanjo, K.Z., Hirata, N., Obara, K. & Kasahara, K., 2012. Decade-scale decrease in b value prior to the M9-class 2011 Tohoku and 2004 Sumatra quakes, *Geophys. Res. Lett.,* **39,** L20304, doi:10.1029/2012GL052997.

National Earthquake Information, Center, 1999. *Preliminary Determination of Epicenters, Monthly Listings,* U.S. Geological Survey, U.S. Dep. of the Interior, Denver, Colo.

Nishenko, S.P., 1985. Seismic potential for large and great earthquakes along the Chilean and southern Peruvian margins of South America: a quantitative reappraisal, *J. geophys. Res.,* **90**(B5), 3589–3615.

Nishenko, S.P., 1991. Circum-Pacific seismic potential, 1989–1999, *Pure appl. Geophys.,* **135**(2), 169–259.

Poli, P., Jeria, A.M. & Ruiz, S., 2017. The Mw 8.3 Illapel earthquake (Chile): preseismic and postseismic activity associated with hydrated slab structures, *Geology,* **45**(3), 247–250.

Pritchard, M.E. & Simons, M., 2006. An aseismic slip pulse in northern Chile and along-strike variations in seismogenic behavior, *J. geophys. Res.,* **111,** B08405, doi:10.1029/2006JB004258.

Rong, Y., Jackson, D.D. & Kagan, Y.Y., 2003. Seismic gaps and earthquakes, *J. geophys. Res.,* **108**(B10), 2471, doi:10.1029/2002JB002334.

Ruegg, J.C. *et al.*, 1996. The Mw = 8.1 Antofagasta (North Chile) earthquake of July 30, 1995: first results from teleseismic and geodetic data, *Geophys. Res. Lett.,* **23**(9), 917–920.

Ruegg, J.C. *et al.*, 2009. Interseismic strain accumulation measured by GPS in the seismic gap between Constitucion and Concepcion in Chile, *Phys. Earth planet. Inter.,* **175,** 78–85.

Scholz, C.H., 1990. *The Mechanics of Earthquakes and Faulting,* Cambridge Univ. Press, 439 pp.

Scholz, C.H., 1998. Earthquakes and friction laws, *Nature,* **391,** 37–42.

Schorlemmer, D., Wiemer, S. & Wyss, M., 2005. Variations in earthquake-size distribution across different stress regimes, *Nature,* **437,** 539–542.

Schurr, B. *et al.*, 2014. Gradual unlocking of plate boundary controlled initiation of the 2014 Iquique earthquake, *Nature,* **512**(7514), 299–302.

Stein, R.S., 1999. The role of stress transfer in earthquake occurrence, *Nature,* **402,** 605–609.

Storchak, D.A., Di Giacomo, D., Bondár, I., Engdahl, E.R., Harris, J., Lee, W. H.K., Villaseñor, A. & Bormann, P., 2013. Public release of the ISC-GEM global instrumental earthquake catalogue (1900–2009) - version 4.0, as of 26 Jan., 2017, period 1900 to 2013, *Seismol. Res. Lett.,* **84**(5), 810–815.

Sykes, L.R., 1971. Aftershock zones of great earthquakes, seismicity gaps, and earthquake prediction for Alaska and the Aleutians, *J. geophys. Res.,* **76,** 8021–8041.

Tilmann, F. *et al.*, 2016. The 2015 Illapel earthquake, central Chile: a type case for a characteristic earthquake?, *Geophys. Res. Lett.,* **43**(2), 574–583.

Udías, A., Madariaga, R., Buforn, E., Muñoz, D. & Ros, M., 2012. The large Chilean historical earthquakes of 1647, 1657, 1730, and 1751 from contemporary documents, *Bull. seism. Soc. Am.,* **102**(4), 1639–1653.

Victor, P., Sobiesiak, M., Glodny, J., Nielsen, S.N. & Oncken, O., 2011. Long-term persistence of subduction earthquake segment boundaries: evidence from Mejillones Peninsula, nothern Chile, *J. geophys. Res.,* **116,** B02402, doi:10.1029/2010JB007771.

Wang, Y.-J., Chan, C.-H., Lee, Y.-T., Ma, K.-F., Shyu, J. B.H., Rau, R.-J. & Cheng, C.-T., 2016. Probabilistic seismic hazard assessment for Taiwan, *Terr. Atmos. Ocean. Sci.,* **27**(3), 325–340.

Yue, H., Lay, T., Rivera, L., An, C., Vigny, C., Tong, X. & Báez Soto, J.C., 2014. Localized fault slip to the trench in the 2010 Maule, Chile M_w = 8.8 earthquake from joint inversion of high-rate GPS, teleseismic body waves, InSAR, campaign GPS, and tsunami observations, *J. geophys. Res.,* **119**(10), 7786–7804.

SUPPORTING INFORMATION

Supplementary data are available at *GJI* online.

Figure S1. Comparison of the results for simulated catalogues with and without missing events: (a) The average cumulative distribution (cdf) and (b) the probability density (pdf) function of the recurrence times for 100 synthetic sequences of $M \geq 7$ events occurring within 500 years. The average number of events in each simulation is 114 for complete catalogues (bold lines) and 90 for incomplete ones (thin lines). In the case of incomplete catalogues, earthquakes are removed which occur in the first 350 years in a 1000 km segment of the 3000 km long fault.

Figure S2. Analysis of the observational catalogue, where magnitudes of events occurring before 1950 are increased by an increment of dM: (a) The cumulative number of $M_w \geq 7.0$ (bluish lines) and $M_w \geq 8.0$ (reddish lines) events as function of time. The vertical dashed line refers to the starting time for the analysis of the $M_w \geq 7.0$ data set. (c) Cumulative frequency-magnitude distribution for the two time periods $T = 200$ years (bluish curves) and 500 years (grey curves). The red dashed line and shaded area refer to a Gutenberg-Richter distribution with $b = 0.7$ and plus/minus one standard deviation.

Figure S3. Corresponding plot to the manuscript Fig. 4, but now for catalogues where the magnitude values of earthquakes before 1950 are increased by an increment of dM: The left column shows the cumulative distribution (cdf) and the right column the probability density (pdf) function of the recurrence times, respectively. The grey shaded areas refer to the 90 per cent confidence interval of a Poisson process. The curves refer to the result of the corresponding earthquake catalogue, where the result of the original data is shown by the green line.

supplement_catalog.pdf

Please note: Oxford University Press is not responsible for the content or functionality of any supporting materials supplied by the authors. Any queries (other than missing material) should be directed to the corresponding author for the paper.